



HAL
open science

Metamorphoses of the flow past an obstacle of a resonantly-driven bistable polariton fluid

Vincent Hakim, Simon Pigeon, Amandine Aftalion

► **To cite this version:**

Vincent Hakim, Simon Pigeon, Amandine Aftalion. Metamorphoses of the flow past an obstacle of a resonantly-driven bistable polariton fluid. 2022. hal-03850547

HAL Id: hal-03850547

<https://hal.science/hal-03850547v1>

Preprint submitted on 13 Nov 2022

HAL is a multi-disciplinary open access archive for the deposit and dissemination of scientific research documents, whether they are published or not. The documents may come from teaching and research institutions in France or abroad, or from public or private research centers.

L'archive ouverte pluridisciplinaire **HAL**, est destinée au dépôt et à la diffusion de documents scientifiques de niveau recherche, publiés ou non, émanant des établissements d'enseignement et de recherche français ou étrangers, des laboratoires publics ou privés.

Metamorphosis of the Landau transition in the flow of a resonantly-driven bistable polariton fluid

Vincent Hakim*

*Laboratoire de Physique de l'École Normale Supérieure,
CNRS, École Normale Supérieure, PSL University,
Sorbonne Université, Université Paris-Diderot, Paris, France*

Simon Pigeon†

*Laboratoire Kastler Brossel, Sorbonne Université, CNRS,
École Normale Supérieure, PSL University, Collège de France, Paris, France*

Amandine Aftalion‡

École des Hautes Etudes en Sciences Sociales, Centre d'Analyse et de Mathématique Sociales, UMR-8557, Paris, France.

(Dated: September 18, 2022)

The onset of dissipation in a flowing superfluid has been the subject of numerous investigations. Motivated by recent experiments, we theoretically analyze the analogous phenomenon for a one-dimensional “quantum fluid of light” which is resonantly driven, and exhibits bistability. The flow is found to abruptly change multiple times when the fluid velocity or the potential strength are increased. In contrast to the classical Landau transition to a time-dependent flow, the transitions take place between stationary states and involve the fluid bistability in an essential way.

It is well-known since the classical analysis of Landau that superfluids exhibit a critical velocity at which dissipation sets in. The discovery of Bose-Einstein condensation in cold atomic vapors has allowed detailed studies of superfluidity [1]. The Landau transition and defect emission in the flow past an obstacle have been experimentally observed with the creation of vortices [2], or gray solitons in a one-dimensional setting [3]. It is well-described theoretically in the framework of the Gross-Pitaevskii equation [4–8]. Beyond cold atomic vapors, exciton-polariton fluids are attracting significant attention [9], as solid-state devices with a higher condensation temperature allowed by the exciton-polariton very low mass. Bose-Einstein condensation has been achieved in these “quantum fluids of light” [9–11] and superfluidity has been studied numerically [12] and experimentally [13, 14], including the nucleation of vortices at a critical flow velocity in the wake of an obstacle [14]. Polaritons are composite bosons that result from the strong coupling between the excitonic resonance of a semiconductor quantum well and a microcavity electromagnetic field [9]. In early experiments, the driving field needed to create polaritons was used either transiently [13] or in a spatially localized way [14] to avoid interfering with the superfluid behavior. The short polariton lifetime then restricts the experiment duration or limits the observations to a local region around the pumping spot. In order to bypass these limitations, it is useful to introduce a support field away from the strong pumping spot used to create the polaritons [15]. This new coherently driven regime has started to be investigated theoretically [11, 15–18] and experimentally [19–22]. The quasi-resonant drive tends to lock the phase of the condensate but when the support field is not too strong, it nonetheless allows the formation

of vortices [20] and dark solitons [21, 22]. However, the dynamical properties of this driven-dissipative condensate and their dependence on the fluid bistable character [23] remain to be better understood [15, 20–22].

Here, we analyze the flow past an obstacle of a resonantly forced condensate in the bistable regime [11, 15, 17, 20–22]. We focus on the one-dimensional case which is the easiest to theoretically analyze. We find, as for conventional superfluids, that a sudden flow change can occur in the wake of the obstacle when the fluid velocity is increased or, when the obstacle strength is increased at fixed velocity. However, the characteristics of this transition and of the resulting flow are found to be quite different from the Landau transition of a superfluid and depend in an essential way on the fluid bistability.

We consider the fluid described by the following generalized Gross-Pitaevskii equation (GGPE)

$$i\hbar\partial_t\psi = \frac{-\hbar^2}{2m}\partial_x^2\psi + \left[V(x) - \hbar\Delta - i\frac{\hbar\gamma}{2} + g|\psi|^2 \right] \psi + F e^{ik_p x}. \quad (1)$$

In the context of exciton-polariton microcavity physics, Eq. (1) provides an effective description of a driven lower polariton field [9, 11], with the polariton-polariton repulsive interaction accounted by the constant $g > 0$. Additional terms as compared to the usual GPE arise from the coherent drive and dissipation [9, 11]. Quasi-resonant pumping is characterized by its amplitude F , its momentum k_p , produced by a slight tilt of the driving laser beam with respect to the cavity plan and by the detuning Δ between the frequency of the driving field and the bottom of the lower polariton band. Dissipation is described by the rate $\gamma > 0$ arising from the polariton finite lifetime. The potential $V(x)$ models a localized obstacle. It is our

main aim to characterize its effect on the fluid flow described by Eq. (1). It is worth noting that our results are also relevant for nonlinear optics where Eq. (1) is known as the Lugiato-Lefever equation [24] and describes wave evolution in a cavity filled with a nonlinear medium (see e.g. [25] and ref. therein).

The explicit x -dependence in Eq. (1) can be eliminated by defining

$$\psi = \sqrt{\hbar\gamma/2g} \phi(x) \exp(ik_p x) \quad (2)$$

The function ϕ then obeys the equation

$$i\partial_\tau \phi = -\frac{1}{2}\partial_{yy}\phi - ik_0\partial_y\phi - [\delta(y) + i - |\phi|^2]\phi + f \quad (3)$$

where we have introduced the dimensionless variables $y = x\sqrt{m\gamma/2\hbar}$, $\tau = t\gamma/2$, and constants, $k_0 = k_p\sqrt{2\hbar/m\gamma}$, $f = F\sqrt{g}(2/\hbar\gamma)^{3/2}$, and defined the function

$$\delta(y) = \delta_0 - \frac{2}{\hbar\gamma}V(y), \text{ with } \delta_0 = \frac{2}{\hbar\gamma} \left[\hbar\Delta - \frac{(\hbar k_p)^2}{2m} \right] \quad (4)$$

Before considering the effect of a localized obstacle, we briefly recall some properties of the fluid described by Eq. (3). When $V(y) = 0$ and $\delta(y) = \delta_0$, Eq. (3) has constant solutions in space and time with a homogeneous density $\rho = |\phi|^2$ which can readily be seen to simply obey,

$$B(\rho) := [(\rho - \delta_0)^2 + 1]\rho = f^2 \quad (5)$$

Two cases can be distinguished. When $\delta_0 < 0$, the function $B(\rho)$, defined in Eq. (5), is obviously monotonically increasing from 0 to ∞ with the density. As a consequence, the density ρ is an increasing function of the forcing amplitude f . When $\delta_0 > 0$, $B(\rho)$ can be non-monotonic with multiple homogeneous solutions for a given forcing. A simple analysis of Eq. (5) shows that this actually happens when $\delta_0 > \sqrt{3}$. An example of this S-like dependency of the density with the driving field is plotted in Fig. 1a-insert and leads to bistability in a window of intermediate forcing strengths i.e. for $B(\rho_+) < f^2 < B(\rho_-)$ with $\rho_\pm = \frac{1}{3} \left(2\delta_0 \pm \sqrt{\delta_0^2 - 3} \right)$. This bistability for sufficiently strong blue detuning is well-known in nonlinear optics [9] and has been demonstrated for polaritons in microcavities [23]. While in the low-density (LD) regime self-interactions are unimportant, the high-density (HD) regime with strong self-interaction allows the observation of superfluidity [26] in a polariton fluid.

Having recalled the basic features of the homogeneous state, we proceed and describe our simulations of Eq. (3) with a localized repulsive ($V(y) > 0$) gaussian potential

$$V(y) = \frac{\hbar\gamma}{2} u_m \exp[-(y/\sigma)^2] \quad (6)$$

We focus on the bistable parameter regime with $\delta_0 > \sqrt{3}$ and the forcing f in the appropriate intermediate interval

(see Fig. 1a). The fluid density is set on the HD state upstream of the obstacle. In an experimental setting, this would result from a strong driving field in a far upstream local region, as proposed in [15] and experimentally realized in e.g. [21]. For a low potential amplitude, the flow is steady, with the density decreasing as expected in the region of the repulsive potential, and returning smoothly to the HD state in the wake of the obstacle, as shown in Fig. 1a. An increase in the potential amplitude u_m produces a transition in the flow, as shown in Fig. 1b, reminiscent of the usual onset of dissipation in a flowing superfluid. However, the character of the transition appears to be very different from the classical Landau transition. Instead of the repeated emission of gray solitons in one dimension [3, 5], the flow restabilizes after a transient. It results again in a stationary flow but with the fluid density in the LD state downstream of the obstacle, as shown Fig. 1b. In other words, for the driven-dissipative GGPE, the critical velocity signals a metamorphosis of the steady flow instead of the appearance of a time-dependent flow. That the flow density downstream of the obstacle lies in the LD state provides a first hint that fluid bistability is playing a significant role in the observed transition. This is further suggested by the fact that, as in previous works [15, 21], a transition is not observed when the driving amplitude f is strong enough for the fluid to be in the monostable HD regime i.e. when $f > f_+$ in Fig. 1a. Simulations performed for potential amplitudes very close to the transition (Fig.1c,d) allow one to better see how the metamorphosis of the steady flow pattern is taking place. When the amplitude of the potential is close to, but below, the critical potential amplitude, the obstacle is followed by a fluid region close to the intermediate density (ID) unstable state (Fig.1c). This region terminates by a front that joins the ID state to the more downstream *HD state*. As the critical potential amplitude is varied and the critical amplitude is approached, this front stands farther and farther downstream from the obstacle, with an increasing region of the fluid downstream of the obstacle in the unstable ID state. For potential with an amplitude slightly greater than the critical one, the complementary process is observed, as shown in Fig.1d. As for subcritical potentials, the obstacle is followed by a fluid region in the unstable ID state but which terminates by a front joining it to the stable *LD state*. With increasing potential amplitude, this front stands closer to the obstacle. It reaches the obstacle and disappears, as soon as the potential amplitude departs by a small amount from the critical one. An important conclusion from these observations is that the critical solution is such that the fluid downward wake exactly stands at the unstable ID state.

In order to more fully understand this transition and the role of bistability in the stationary flow metamorphosis, we consider the parameter regime suitable for theoretical analysis, provided by an obstacle that varies on a

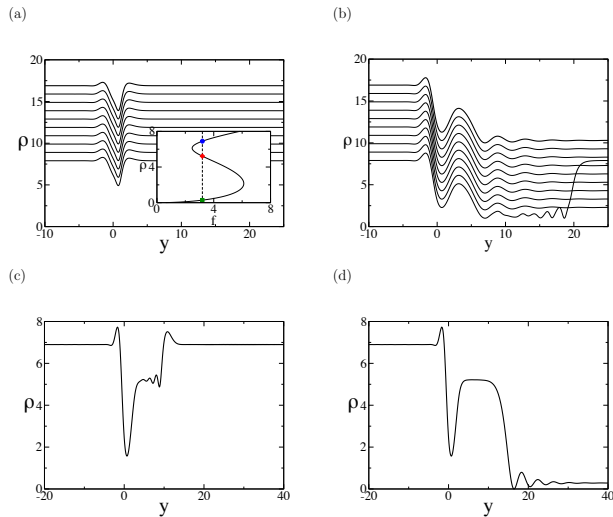


FIG. 1: Numerical simulations of Eq. (3). (a) Insert : fluid density ρ vs. forcing f as described by Eq. (5). In the parameter regime considered, there are three homogeneous steady states, stable HD (solid blue circle) and LD states (solid green square) as well as an unstable ID one (solid red diamond). (a)& (b) The fluid is injected in the HD state. The curves represent the fluid density at different times and have been shifted with time to highlight the stationarity of the flow. (a) for a small potential amplitude $u_m = 2$, the flow is steady and is in the HD state in the wake of the obstacle at $y \gg 0$. (b) For a larger $u_m = 6$, the flow is still stationary, but is in the LD in the wake of the obstacle. (c)&(d)Detail of the transition. (c) $u_m = 5.50$ (d) $u_m = 5.501$ (see the main text for a discussion). Other parameters are $\delta_0 = 6.2$, $f = 3.2$, $k_0 = 2.75$ which corresponds to the typical experimental values $\hbar\Delta = 0.5\text{MeV}$, $\hbar\gamma = 0.1\text{MeV}$, $\hbar^2/m = 1\text{MeV}\mu\text{m}^2$, $k_p = 0,616\mu\text{m}^{-1}$, $\sqrt{g}F = 0.036(\text{MeV})^{3/2}$. The potential range is $\sigma = 1$ corresponding to $4.5\mu\text{m}$, the chosen unit length.

long length scale, $\sigma \gg 1$ (Eq. (6)). For a slowly varying obstacle, when the flow is accordingly slowly varying, the derivative terms in Eq. (3) can be treated perturbatively. At the lowest order, they can be entirely neglected and the “adiabatic” solution, $\phi_a(y) = \sqrt{\rho_a(y)} \exp[i\theta_a(y)]$, readily obtained. The fluid density ρ_a , is linked to the potential amplitude by Eq. (5) with δ_0 simply replaced by $\delta(y)$ (Eq. (4)), which takes into account the influence of the potential on the detuning. In this adiabatic approximation, solving the quadratic Eq. (5) for $\delta(y)$ provides the implicit relation between the fluid density and the potential,

$$\delta(y) = \rho_a(y) \pm \sqrt{\frac{f^2}{\rho_a(y)} - 1}, \quad 0 \leq \rho_a \leq f^2. \quad (7)$$

As for homogeneous solutions, the solution phase is sim-

ply given as a function of the density

$$\theta_a(y) = \arctan\left(\frac{1}{\rho_a(y) - \delta(y)}\right) \quad (8)$$

The relation (7) between the density and δ at fixed forcing amplitude f , is plotted in Fig. 2a. It is equivalent but more convenient for our purpose than the insert of Fig. 1a, which gives the density as a function of f for fixed “detuning” δ . A simple calculation shows that Eq. (7) determines the density as a unique function of $\delta(y)$ when $f < f_c = (4/3)^{3/4} \simeq 1.2408$ while for $f > f_c$, there is a range of δ values with multiple possible densities. In other words, bistability occurs for a range of δ values when $f > f_c$, as illustrated in Fig. 2a.

Let us now consider, a fluid injection in the HD state, when the forcing is sufficiently strong for bistability to occur (i.e. $f > f_c$). As the potential varies with the position y , $\delta(y)$ follows it according to Eq. (4). The density, as given by Eq. (7), moves along the HD branch in Fig. 2a. The adiabatic solution is already a close approximation of the flow obtained by numerically solving Eq. (3), for the gaussian potential of Eq. (6) even with a rather large amplitude ($u_m = 6$) when $\sigma = 4$ (Fig. 2b).

We first briefly describe the case of an *attractive* potential ($u_m < 0$). Eq. (7) predicts that the fluid density goes up the high density branch as $V(y)$ becomes more negative. The flow should undergo a transition if u_m is large enough for the top of the high density branch to be reached, since the branch cannot be followed beyond its top. This transition is indeed confirmed in numerical simulations of Eq. (3) (Fig. S1). As for repulsive potentials, when $|u_m|$ is larger than the critical one, the flow is stationary and, above the transition the fluid density in the wake of the obstacle is in the LD state.

How a transition can happen for a *repulsive* potential ($u_m > 0$) is less obvious. The density of the adiabatic solution (Eq. (7)) follows the high density branch toward low density before increasing again in the wake of the obstacle, as shown in Fig. 2a. This appears a smooth process for all potential strengths u_m . It is not clear why this would result in a transition of the flow profile at a critical amplitude u_m and what this critical amplitude would be. In particular, no hint is provided by computing linear (i.e. Bogoliubov) excitations [18, 19] around the local homogeneous fluid density. However, one can note that in the adiabatic approximation, all derivatives are absent and, as a consequence, the fluid velocity plays no role. This suggests to go beyond the adiabatic approximation and treat perturbatively the derivatives terms. Writing $\rho(y) = \rho_a(y) + \rho_1(y) + \dots$, $\theta(y) = \theta_a(y) + \theta_1(y) + \dots$, the first corrections to the adiabatic solution of Eq. (7), (8) are obtained after a short calculation as,

$$\rho_1(y) = -\frac{2k_0}{B'(\rho_a)} \frac{d\rho_a}{dy}, \quad \theta_1(y) = \frac{k_0}{B'(\rho_a)} \frac{d[\delta(y) - 2\theta_a]}{dy} \quad (9)$$

where the function $B(\rho)$ is defined in Eq. (5). These corrections are shown in Fig. 2b and, as expected, they result in a closer agreement between the analytic approximations and the numerical profiles. More interestingly, the corrected density profile in the (ρ, b) diagram provides a clue to the origin of the instability (Fig. 2a). One observes that the correction (9) produces a departure of the profile from the high density branch towards the middle unstable branch when the potential returns to 0, in the close downward wake of the obstacle. Eq. (9) shows that this non-adiabatic effect grows with k_0 and, it also grows with the localized potential amplitude u_m . One can therefore guess, that, for sufficiently large u_m or k_0 , this leads the flow profile loop in Fig. 2a, to reach the unstable density branch in the (ρ, b) diagram and lead to an instability. While suggestive, this argument is obviously not rigorous since the perturbative correction (9) cannot be trusted when it provides a significant correction to the lowest order result.

In order to obtain a full reduced nonlinear description, a further asymptotic limit is needed, beyond that of a slowly varying potential (i.e. $\sigma \rightarrow \infty$). A simple mathematical one is obtained by increasing the flow velocity k_0 at the same time as the length scale of the potential is varied, i.e. taking the limit, $\sigma \rightarrow \infty$, $k_0 \rightarrow \infty$ with a fixed ratio $\kappa = k_0/\sigma$. Determining the steady solution of Eq. (3) reduces in this limit to solving the simple system,

$$\kappa \partial_z \rho = -2\rho - 2f\sqrt{\rho} \sin(\theta) \quad (10)$$

$$\kappa \partial_z \theta = [\delta(z) - \rho] - f \cos(\theta)/\sqrt{\rho} \quad (11)$$

where $z = y/\sigma$. Eq. (10), (11) simply give back for $\kappa = 0$ the adiabatic solution (7),(8) and, perturbatively for small κ , the correction (9). But, in the asymptotic limit considered, κ can now take any value. The reduced system (10),(11) has only first-order derivatives in z . Its phase-plane can be easily determined (Fig. S2). Eq. (10), (11) have only one spatially-divergent modes from the unstable ID at $z = +\infty$. A simple shooting method determines the amplitude of the potential for which this divergence vanishes and the solution tends at $z = +\infty$ toward the ID branch, as illustrated in Fig. 3a. It brings however a surprise : for given driving parameters, multiple transitions are found by increasing the localized potential amplitude. The fluid density in the wake of the obstacle is in the HD state for low potential amplitudes. At a first critical amplitude, it jumps to the LD state, as described above. When the potential amplitude is further increased, a second transition is found, at which the fluid density jumps back to the HD state. Further transitions are found for still higher values of u_m . The loci of these transitions are plotted in the (k_0, u_m) parameter plane in Fig. 3b.

These multiple solutions and the asymptotics of the $u_m^*(k_0)$ branches can be understood by considering Eq. (10), (11) for large κ . In this limit, the evolution

of ρ and θ with z is slow, except for the potential term $\delta(z)$ that evolves on a z -scale of order 1. The density of a solution of Eq. (10), (11), that starts in the HD state at $z = -\infty$, does not significantly change when it encounters the localized potential while its phase rotates by an angle $\Delta\theta$,

$$\Delta\theta = -\frac{2}{\hbar\gamma\kappa} \int_{-\infty}^{+\infty} dz V(z) = -\sqrt{\pi} u_m/\kappa \quad (12)$$

where the second equality holds for the Gaussian potential (6). For the solution to end up at $z = +\infty$ in the ID state, the phase turn $\Delta\theta$ has to bring it precisely, on one of the two entering separatrices of the ID unstable state, as shown in Fig. S2. Namely, $\Delta\theta$ should be equal to $\Delta\theta_{1,2} - 2n\pi$, $n = 0, 1, \dots$ with $\theta_1 \simeq -1.844$, $\theta_2 \simeq -4.464$ for the parameter values of Fig. 3c. The angle values with $n \geq 1$ correspond to the solution phase making full rotations before reaching one of the two separatrices. The double series of critical potential amplitudes follows from Eq. (12),

$$u_m = -\kappa (\theta_{1,2} - 2n\pi)/\sqrt{\pi}, \quad n = 0, 1, 2, \dots \quad (13)$$

Eq. (13) shows that asymptotically u_m depends linearly on $\kappa = k_0/\sigma$. The slopes given by Eq. (13) for the three lowest branches are displayed in Fig. 3b together with the numerically obtained solutions. The two lowest transition branches merge at $\kappa \simeq 1.30$. The 4th and higher branches cross and recombine at intermediate κ values, producing the bifurcation diagram shown in Fig. 3b.

The bifurcation diagram of Fig. 3b holds for the reduced asymptotic problem (Eq. (10,11)). We have checked that away from this asymptotic limit, similar diagrams are obtained for the GGPE with our reference parameters (Fig. S3). For potential range $\sigma = 1$ or 2, three transitions are observed upon increase of the local potential strength u_m for large enough k_0 (e.g. $k_0 = 6.2$ for $\sigma = 2$) and no transitions are observed for small enough k_0 [28].

In conclusion, we have found that the drive provided by a constant support field deeply changes the Landau transition. The stationary flow profile undergoes a metamorphosis instead of becoming time-dependent. Moreover, for given flow and pumping parameters, successive transitions exist at a discrete number of potential amplitudes. We have shown that these phenomena can be described and understood analytically in suitable asymptotic regimes. These results certainly suggest a careful reexamination of the Landau transition in higher dimensions. We also hope that they will motivate experimental studies of the phenomenon. Finally, we cannot help but wonder, whether the extended switches of the fluid density wake induced by a localized obstacle could provide useful applications in all-optical technology and devices [27].

Acknowledgments. We would like to thank A. Bramati and E. Giacobino for instructive discussions.

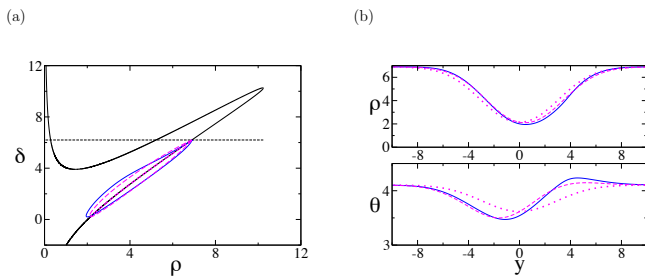


FIG. 2: Adiabatic approximation and corrections. (a) Plot in the (ρ, b) diagram. (b) Plot of the density and the phase vs. y . The stationary numerical solution (solid blue) of Eq. (3) is plotted together with the adiabatic solution alone (dotted magenta; Eq. (7),(8)) or with the first-order corrections (dashed magenta; Eq. (9)). The parameters are $\sigma = 4$, $u_m = 6$, $k_0 = 2.75$, $f = 3.2$, $\delta_0 = 6.2$.

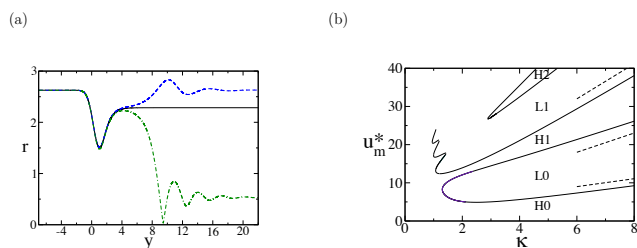


FIG. 3: Reduced asymptotic description. (a) Solutions of Eq. (10,11) for $\kappa = 2.75$. In the obstacle wake, the flow tends towards the HD state for $u_m = 4.9$ (dashed blue) and toward the LD state for $u_m = 5.0$ (dashed-dotted green). The critical flow corresponds to $u_m^* \simeq 4.93$ (solid dark) and tends to the ID state. (b) Diagram of the transition lines in the (κ, u_m) plane. The asymptotic slopes for large κ of the three lowest transition lines given by Eq. (13) are shown (dashed). In the different parameter regions, it is indicated whether the flow in the wake of the obstacle tends toward the high (H) or the low (L) density states with the numbers corresponding to the additional 2π dephasing (Eq. (13)) of the large κ solutions in their downstream wake, as compared to the H0 and L0 ones. At finite κ the different regions of the same type with different numbers (e.g. H0 and H1) are delimited by nodal lines of solutions (not shown) with vanishing density at a point allowing the required phase jump. The zigzagging transition line at $\kappa \simeq 1$ has only been computed up to $u_m^* = 24$. The other parameters are $f = 3.2$, $\delta_0 = 6.2$.

* Electronic address: vincent.hakim@ens.fr

† Electronic address: simon.pigeon@lkb.upmc.fr

‡ Electronic address: amandine.aftalion@ehess.fr

[1] L. Pitaevskii and S. Stringari, *Bose-Einstein condensation and superfluidity*, vol. 164 (Oxford University Press, 2016).

[2] C. Raman, M. Köhl, R. Onofrio, D. Durfee, C. Kuk-

lewicz, Z. Hadzibabic, and W. Ketterle, *Physical Review Letters* **83**, 2502 (1999).

[3] P. Engels and C. Atherton, *Physical Review Letters* **99**, 160405 (2007).

[4] T. Frisch, Y. Pomeau, and S. Rica, *Physical Review Letters* **69**, 1644 (1992).

[5] V. Hakim, *Physical Review E* **55**, 2835 (1997).

[6] B. Jackson, J. McCann, and C. Adams, *Physical Review A* **61**, 013604 (1999).

[7] C. Huepe and M.-E. Brachet, *Physica D: Nonlinear Phenomena* **140**, 126 (2000).

[8] A. Aftalion, Q. Du, and Y. Pomeau, *Physical Review Letters* **91**, 090407 (2003).

[9] I. Carusotto and C. Ciuti, *Reviews of Modern Physics* **85**, 299 (2013).

[10] J. Kasprzak, M. Richard, S. Kundermann, A. Baas, P. Jeambrun, J. M. J. Keeling, F. Marchetti, M. Szymańska, R. André, J. Staehli, et al., *Nature* **443**, 409 (2006).

[11] I. Amelio and I. Carusotto, *Physical Review B* **101**, 064505 (2020).

[12] S. Pigeon, I. Carusotto, and C. Ciuti, *Phys. Rev. B* **83**, 144513 (2011).

[13] G. Nardin, G. Grosso, Y. Léger, B. Pietka, F. Morier-Genoud, and B. Deveaud-Plédran, *Nature Physics* **7**, 635 (2011).

[14] A. Amo, S. Pigeon, D. Sanvitto, V. Sala, R. Hivet, I. Carusotto, F. Pisanello, G. Leménager, R. Houdré, E. Giacobino, et al., *Science* **332**, 1167 (2011).

[15] S. Pigeon and A. Bramati, *New Journal of Physics* **19**, 095004 (2017).

[16] I. Chestnov, A. Kavokin, and A. Yulin, *New Journal of Physics* **21**, 113009 (2019).

[17] S. Pigeon and A. Aftalion, *Physica D: Nonlinear Phenomena* **415**, 132747 (2021).

[18] M. Joly, L. Giacomelli, F. Claude, E. Giacobino, Q. Glorieux, I. Carusotto, A. Bramati, and M. J. Jacquet, arXiv preprint arXiv:2110.14452 (2021).

[19] P. Stepanov, I. Amelio, J.-G. Rousset, J. Bloch, A. Lemaître, A. Amo, A. Minguzzi, I. Carusotto, and M. Richard, *Nature communications* **10**, 1 (2019).

[20] S. Koniakhin, O. Bleu, D. Stupin, S. Pigeon, A. Maître, F. Claude, G. Lerario, Q. Glorieux, A. Bramati, D. Solnyshkov, et al., *Physical Review Letters* **123**, 215301 (2019).

[21] G. Lerario, A. Maître, R. Boddeda, Q. Glorieux, E. Giacobino, S. Pigeon, and A. Bramati, *Physical Review Research* **2**, 023049 (2020).

[22] A. Maître, G. Lerario, A. Medeiros, F. Claude, Q. Glorieux, E. Giacobino, S. Pigeon, and A. Bramati, *Physical Review X* **10**, 041028 (2020).

[23] A. Baas, J. P. Karr, H. Eleuch, and E. Giacobino, *Physical Review A* **69**, 023809 (2004).

[24] L. A. Lugiato and R. Lefever, *Physical Review Letters* **58**, 2209 (1987).

[25] P. Parra-Rivas, E. Knobloch, D. Gomila, and L. Gelens, *Physical Review A* **93**, 063839 (2016).

[26] A. Amo, J. Lefrère, S. Pigeon, C. Adrados, C. Ciuti, I. Carusotto, R. Houdré, E. Giacobino, and A. Bramati, *Nature Physics* **5**, 805 (2009).

[27] D. Ballardini *et al.*, *Nature communications* **4**, 1 (2013).

[28] Eq. (13) actually holds exactly for the GGPE in the large k_0 and large u_m limit for potentials of finite range.

Supplementary figures

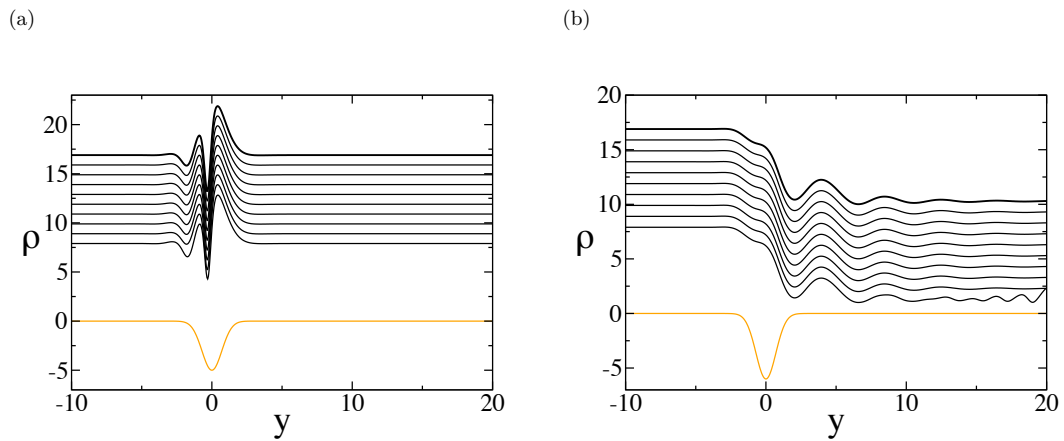


FIG. S1: Transition in the GGPE for an *attractive* potential. Simulations for two localized potential amplitudes (a) $u_m = -5$ (b) $u_m = -6$. The density is shown at different times is (solid black line). The curves have been shifted upward with time to show the stationarity of the flow. Note that the fluid beyond the obstacle is in the HD state in (a) and in the LD state in (b). The attractive localized potential is also shown (orange solid line). The other parameters are $f = 3.2$, $\delta_0 = 6.2$, $k_0 = 2.75$, $\sigma = 1$.

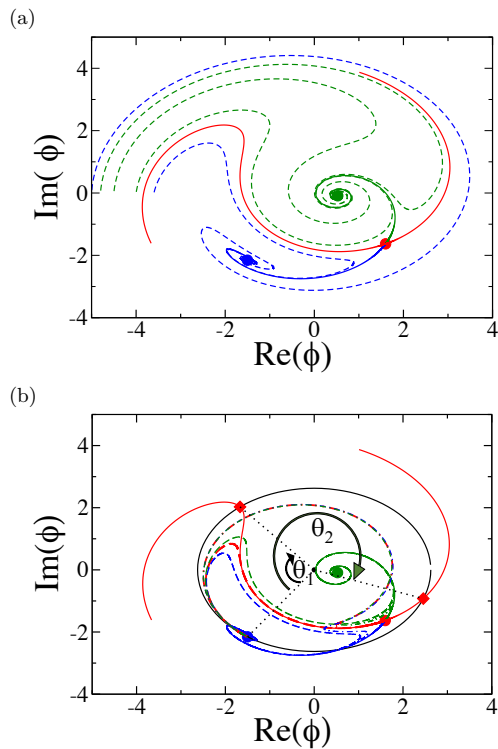


FIG. S2: Phase plane analysis of the reduced asymptotic problem. (a) Phase plane of the homogeneous problem (Eq. (10,11)) (i.e. without the localized potential) showing the three fixed points, HD (blue solid disk), ID (red solid disk), LD (green solid disk) together with the two entering separatrices (red solid lines) of the ID fixed point and the outgoing ones, ending on the HD point (blue solid line) or the LD point (green solid line). Several trajectories are also shown ending either on the HD point (dashed blue line) or the LD point (dashed green line). (b) Same diagram as (a) but showing two critical trajectories of the reduced problem for $\kappa = 6.0$ with the localized gaussian potential of amplitude $u_{m,1}^* \simeq 7.328$ (dashed red line) and $u_{m,2}^* \simeq 21.34$ (dashed-dotted red line), corresponding to the first two transitions when u_m is increased from 0. The critical trajectories start in the HD fixed point and they end on the ID fixed point. For each of these transition points, two other trajectories are shown which end either at the HD point, with $u_m = 6.5 < u_{m,1}^*$ (dashed blue line) and $u_m = 21.8 > u_{m,2}^*$ (dashed-dotted blue line), or at the LD point, with $u_m = 8.0 > u_{m,1}^*$ (dashed green line) and $u_m = 21.0 < u_{m,2}^*$ (dashed-dotted green line). It is also shown a circle of radius equal to the modulus of the HD point (solid black line) centered at the origin (solid black circle) as well as its intersections (red diamond) with the entering separatrices of the ID point. The phase difference θ_1 and θ_2 between these intersection points and the HD point are indicated. They provide the asymptotic slopes of the different transition branches (see Eq.(13) and the main text). The other parameters are $f = 3.2$, $\delta_0 = 6.2$.

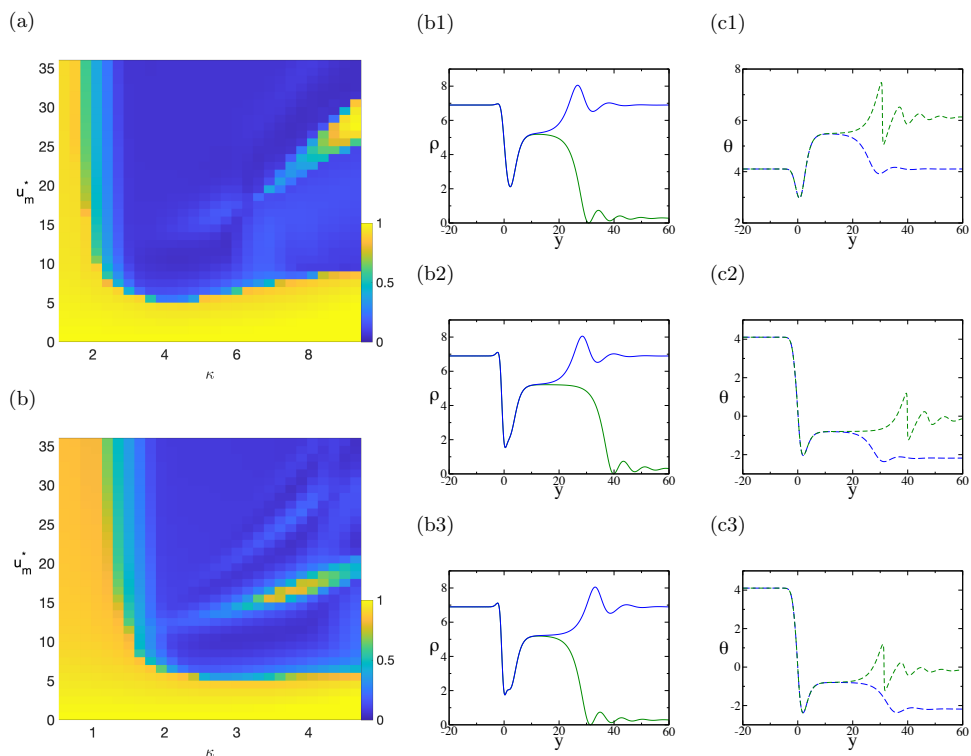


FIG. S3: Results of simulations of the GGPE (Eq. (3)) for $f = 3.2, \delta_0 = 6.2$ for different values of the localized potential amplitude u_m and momentum $\kappa = k_0/\sigma$. The fluid is injected in the HD state at $y \ll 0$. (a)&(b) The potential range is $\sigma = 1$ in (a) and $\sigma = 2$ in (b). The color code indicates the relative density in the wake of the obstacle relative to the density in the HD state. Flow in the HD state downstream of the obstacle (yellow) correspond to states marked H in Fig. 3b of the main text for the reduced model. Flow in the LD state downstream of the obstacle (dark blue) corresponds to states marked L in Fig. 3b. Intermediate colors are due to the limited resolution of the numerical procedure used to scan this two-parameter plot. The figures correspond rather closely to Fig. 3b although σ is not large. A difference is that the band H1 terminates and does not exist at low κ values, presumably due to the recombination of the 2nd (H0→L1) and 3rd transition (H1→L1). For higher values of κ , the transition lines are close to that of the reduced model. (b)&(c) Close-up on 3 transitions with increasing u_m with higher resolution, at $k_0 = 6.2$ and $\sigma = 2$. Solution densities ((b), solid lines) and phases ((c), dashed lines) are shown for two values of the potential just below and just above the transition. The fluid in the obstacle wake is either in the HD state (blue) of the LD state (green). (b1) & (c1) 1st transition with $u_m = 4.85$ (HD state) and $u_m = 4.86$ (LD state) (b2) & (c2) 2nd transition with $u_m = 14.16$ (LD state) and $u_m = 14.17$ (HD state). Note that the 2nd transition is inverted as compared to the 1st, namely the fluid density jumps back to the HD state when u_m is increased. While the density at $y \gg 1$ in the HD states are the same in (b1) and (b2), the phase is lower by 2π in (c2) as compared to (c1) in agreement with the asymptotic analysis. The phases of the LD state at $z \gg 1$ also differ by 2π between (c2) and (c1) while for larger k_0 they would be the same as in the asymptotic analysis. This additional phase jump comes from the crossing of a (nodal) line of LD solutions, for which the density vanishes at a point, when increasing u_m in the LD region. (b3) & (c3) 3rd transition with $u_m = 14.84$ (HD state) and $u_m = 14.85$ (LD state). The transition is analogous to the first one, but with the phases shifted by 2π in the far downstream wake of the obstacle.